scientific reports

Check for updates

OPEN

Mechanistic insights into 18β-glycyrrhetinic acid-induced apoptosis in SCC-9 cells revealed by TMT proteomics and network pharmacology

Hongli Fan[1,3], Daichang Yuan[2] & Yi Nan[1,3]✉

18β-Glycyrrhetinic acid (18β-GRA), a major bioactive component of licorice, exhibits recognized biological activities in various tumor models. However, its cellular effects and underlying molecular mechanisms in tongue squamous cell carcinoma (TSCC) are not well characterized. This study aimed to investigate the molecular mechanisms of 18β-GRA against TSCC by integrating quantitative proteomics with network pharmacology. The CCK-8 assay was used to assess cell viability. Cell-cycle distribution and apoptosis were analyzed by flow cytometry. Intracellular Reactive Oxygen Species (ROS) levels were detected using DCFH-DA staining. Tandem Mass Tag (TMT)-based quantitative proteomics was employed to identify differentially expressed proteins, followed by functional enrichment and subcellular localization analyses. Western blotting was performed to examine the expression of proteins associated with apoptosis, autophagy, and the PI3K/AKT pathway. Network pharmacology was applied to predict potential targets of 18β-GRA. Common targets shared with TSCC were mapped onto a protein-protein interaction network, and molecular docking was used to evaluate the binding affinity of 18β-GRA to these overlapping proteins. 18β-GRA significantly inhibited SCC-9 cell viability in a dose- and time-dependent manner and induced G0/G1 phase arrest. The percentages of apoptotic cells and intracellular ROS levels increased with higher concentrations of 18β-GRA. Proteomic analysis revealed widespread alterations in pathways involved in metabolism, cellular structure, apoptosis, and autophagy. Western blotting confirmed upregulation of Bax, downregulation of Bcl-2, an increased LC3-II/LC3-I ratio, decreased p62 expression, and reduced phosphorylation of AKT1. Network pharmacology identified six intersection targets between 18β-GRA and TSCC, which were enriched in metabolic and cancer-related pathways including the PI3K-Akt pathway. Molecular docking suggested stable binding interactions between 18β-GRA and all six candidate proteins. 18β-GRA exerts multi-faceted effects on SCC-9 cells, including growth inhibition, cell-cycle arrest, apoptosis induction, oxidative stress enhancement, and modulation of autophagy markers. The integrated proteomic and computational approach implicates several key pathways and protein targets in the anti-TSCC activity of 18β-GRA, providing a broader molecular context for its mechanistic understanding.

Keywords 18β-Glycyrrhetinic acid, Tongue squamous cell carcinoma, Apoptosis, TMT-based proteomics, Network pharmacology

Tongue squamous cell carcinoma (TSCC) is the most prevalent malignancy of the oral cavity, accounting for nearly 90% of oral cancer cases worldwide. Its incidence has continued to rise in recent years, posing a persistent clinical challenge[1,2]. Tobacco and alcohol consumption are the dominant risk factors for TSCC. However, human papillomavirus (HPV) infection has increasingly been recognized as a significant etiological contributor, particularly among younger patients[3,4]. HPV-positive and HPV-negative TSCC represent distinct

[1]Traditional Chinese Medicine College, Ningxia Medical University, Yinchuan 750004, Ningxia, China. [2]Xianfeng Traditional Chinese Medicine Hospital, Xianfeng 445600, Hubei, China. [3]Key Laboratory of Dryness Syndrome in Chinese Medicine, Ministry of Education, Ningxia Medical University, Yinchuan 750004, Ningxia, China. ✉email: 20080011@nxmu.edu.cn

disease entities. HPV-positive tumors exhibit unique molecular signatures and are generally associated with more favorable clinical outcomes compared to HPV-negative disease, underscoring the significant biological heterogeneity within TSCC[5]. In the present study, we utilized the SCC-9 cell line, a well-characterized model of HPV-negative tongue squamous cell carcinoma, which aligns with investigating a disease subset associated with poorer prognosis and greater therapeutic challenges[5].

Despite advances in diagnostics and therapeutic modalities — including refinements in glossectomy techniques and improvements in postoperative functional reconstruction — the overall survival rates for TSCC have not improved substantially over the past decades[6–8]. Many patients continue to experience long-term morbidity, such as impaired articulation, swallowing dysfunction, and the risk of osteoradionecrosis, highlighting the pressing need for more effective and less debilitating treatment strategies[9,10].

Consequently, research has increasingly focused on elucidating the molecular mechanisms driving TSCC progression. Studies targeting pathways involved in cell-cycle control, apoptosis, metabolic reprogramming, and immune evasion have identified potential avenues for therapeutic intervention. In parallel, natural compounds derived from medicinal plants have gained momentum as promising antitumor agents due to their multi-target regulatory activities (i.e., the ability to concurrently modulate multiple signaling pathways). Several phytochemicals, including ganoderma polysaccharides, shikonin derivatives, salidroside, asiatic acid, honokiol, and ursolic acid, have demonstrated the ability to inhibit proliferation and induce apoptosis in oral squamous carcinoma cells through modulation of ERK, PI3K/AKT, p53, and Bcl-2 family signaling pathways[11–13].

Among these compounds, 18β-glycyrrhetinic acid (18β-GRA)—a major bioactive metabolite of *Glycyrrhiza* species — has attracted considerable interest for its broad anti-inflammatory and antitumor properties[13,14]. Previous studies have demonstrated that 18β-GRA can induce mitochondrial dysfunction, promote reactive oxygen species (ROS) accumulation, and activate caspase-dependent apoptosis in various cancer models, including gastric, lung, breast, and liver cancers[15–17]. Notably, emerging preclinical evidence suggests that 18β-GRA may hold therapeutic potential for head and neck squamous cell carcinomas. Its documented ability to suppress invasion, metastasis, and tumor growth in related models—coupled with its known anti-inflammatory effects that could mitigate treatment-related morbidity — provides a rationale for its investigation in improving therapeutic outcomes and functional recovery in TSCC[18]. However, the specific effects of 18β-GRA on TSCC and its underlying molecular mechanisms remain poorly understood.

Given the multifactorial molecular alterations characterizing TSCC, particularly in aggressive HPV-negative cases, and the multi-pathway regulatory potential of plant-derived compounds like 18β-GRA, it represents a promising candidate for further investigation. Therefore, this study employed the HPV-negative SCC-9 cell line in conjunction with cellular assays, tandem mass tag (TMT)-based quantitative proteomics, network pharmacology, and molecular docking to systematically evaluate the antitumor activity of 18β-GRA and to elucidate the signaling pathways that may mediate its effects.

Materials and methods

Cell culture

The human tongue squamous cell carcinoma cell line SCC-9 (Cat. No. GCC-TO0003; Shanghai GeneChem Co., Ltd., China) was maintained under standard conditions in a humidified incubator at 37 °C with 5% CO_2. Cells were cultured in Dulbecco's Modified Eagle Medium/Nutrient Mixture F-12 (DMEM/F-12) medium (Cat. No. 11330032, Gibco, USA) supplemented with 10% fetal bovine serum (FBS; Cat. No. 1828728, Gibco, USA), 400 ng/mL hydrocortisone, 0.5 mM sodium pyruvate, and 1% penicillin–streptomycin solution (Cat. No. P1400-100, Solarbio, Beijing, China). The medium was refreshed every two days, and cells were passaged while in the logarithmic growth phase. In all experiments, the negative control wells received medium containing 0.05% dimethyl sulfoxide (DMSO), whereas blank wells contained medium only.

Cell viability assay (CCK-8)

SCC-9 cells were seeded in 96-well plates at a density of 5×10^3 cells per well and allowed to adhere for 24 h. To synchronize cell cycles and minimize potential serum interference on drug response, cells were serum-starved in DMEM/F-12 containing 2% FBS for 12 h. Subsequently, cells were treated with 18β-glycyrrhetinic acid (18β-GRA; >97% purity, Sigma-Aldrich, Cat. No. G10105-10G) at concentrations of 40, 80, 120, 160, and 200 μM. Blank control and negative control groups were included in the experiment. This concentration range was selected based on preliminary dose-response experiments and is consistent with effective anti-proliferative ranges reported in prior studies on other cancer cell lines[14]. 18β-GRA was dissolved in DMSO as a 1 mg/mL stock solution and diluted with complete medium immediately before treatment. The final DMSO concentration was maintained at ≤ 0.05% (v/v) in all treatment and control groups. Each condition was assayed in six replicates.

Cell viability was measured using the CCK-8 assay (KeyGEN BioTECH, Cat. No. KGA317, China). At 24, 48, and 72 h post-treatment, the medium was aspirated, and cells were gently washed once with pre-warmed phosphate-buffered saline (PBS) to remove residual compounds. A 1:10 dilution of CCK-8 reagent in phenol red-free medium was added to each well, followed by incubation at 37 °C for 2 h. Absorbance at 450 nm was recorded using a microplate reader (SpectraMax iD3, Molecular Devices, USA). Viability was calculated as follows:

$$\text{Viability } (\%) = [(\text{OD}_{\text{treated}} - \text{OD}_{\text{blank}}) / (\text{OD}_{\text{negative control}} - \text{OD}_{\text{blank}})] \times 100.$$

The half-maximal inhibitory concentration (IC_{50}) at each time point was derived by fitting viability data against log-transformed drug concentrations using a four-parameter logistic (4PL) nonlinear regression model in GraphPad Prism (GraphPad Prism, Version 7.0, URL: https://www.graphpad.com/scientific-software/prism/). The model was constrained where appropriate, and goodness-of-fit was assessed via R^2 values.

Flow cytometry for apoptosis analysis

SCC-9 cells were seeded into six-well plates and allowed to reach approximately 80% confluence. Cells were then exposed to 18β-GRA at final concentrations of 30 μM (low), 60 μM (middle), or 90 μM (high), whereas negative control wells received medium containing 0.05% DMSO. After 48 h of treatment, both the culture supernatant and adherent cells were collected. Cells were detached with trypsin, combined with the corresponding supernatant, and pelleted by centrifugation, followed by two washes with pre-chilled D-Hanks buffer (pH 7.2–7.4).

Cell apoptosis was assessed using the Annexin V-Fluorescein Isothiocyanate (V-FITC)/Propidium Iodide (PI) apoptosis detection kit (Cat. No. KGA107, Jiangsu KGI Biotechnology Co., Ltd., China) following the manufacturer's instructions. Briefly, the cell pellets were resuspended in 500 μL of 1× binding buffer, after which 5 μL Annexin V-FITC and 5 μL PI were added. The samples were then mixed by inverting the tube 5–10 times to ensure complete suspension of cells, followed by incubation for 15 min at room temperature in the dark.

Flow cytometry was performed immediately on a Guava easyCyte HT flow cytometer (Luminex Corporation, USA). An integrated 488 nm laser was used for excitation. Green fluorescence from Annexin V-FITC was collected through a 525/30 nm bandpass filter (BL1 channel), and red fluorescence from PI was collected through a 583/26 nm bandpass filter (BL2 channel). Prior to sample acquisition, instrument performance was verified using Guava CheckBeads, and compensation was automatically calculated by the instrument software (GuavaSoft, Version 3.3, URL: https://www.merckmillipore.com/) using single-stained controls prepared with the kit reagents. For each sample, at least 5,000 events were acquired. Cells were first gated on a forward scatter (FSC) versus side scatter (SSC) dot plot to exclude debris. Apoptotic populations were then quantified from this live-cell gate: viable cells (Annexin V^-/PI^-), early apoptotic cells (Annexin V^+/PI^-), late apoptotic cells (Annexin V^+/PI^+), and necrotic cells (Annexin V^-/PI^+).

Cell-cycle analysis

Upon reaching approximately 80% confluence in six-well plates, SCC-9 cells were exposed to 18β-GRA at final concentrations of 30 μM (low), 60 μM (middle), or 90 μM (high), whereas negative control wells received medium containing 0.05% DMSO. After 48 h of treatment, cells were harvested by trypsinization, washed with phosphate-buffered saline (PBS), and fixed overnight at 4 °C in pre-cooled 70% ethanol (v/v, in distilled water). Following fixation, the ethanol was removed by washing with PBS, and each sample was incubated with 500 μL of propidium iodide (PI)/RNase A staining solution, prepared according to the manufacturer's instructions for the Cell Cycle Detection Kit (Cat. No. KGA512, Jiangsu KeyGEN BioTECH Corp., Ltd., China; PI: RNase A volume ratio = 1:9). The samples were stained in the dark at room temperature for 30 min. Cell cycle distribution was analyzed using a flow cytometer with excitation at 488 nm and emission collected through a 575/20 nm bandpass filter, corresponding to the peak fluorescence emission of PI. All experiments were performed following the manufacturer's protocol and established methods in the field[15].

Measurement of intracellular ROS levels

Following attachment, SCC-9 cells in six-well plates were treated with 90 μM 18β-GRA (high group) or a negative control (0.05% DMSO) for 48 h. Cells were then washed with PBS and incubated with 10 μM DCFH-DA (Beyotime Biotechnology, Cat. No. S0033S, China) in serum-free medium for 30 min at 37 °C in the dark, with gentle agitation every 10 min. After removing the probe and washing with PBS, intracellular ROS levels were immediately measured by flow cytometry using the FITC channel. Data analysis was based on three independent biological replicates.

Quantitative real-time PCR (qPCR) analysis

SCC-9 cells were treated with 90 μM 18β-GRA (high group) or negative control (0.05% DMSO) for 48 h. Total RNA was then extracted using TRIzol Reagent (Invitrogen, Cat. No. 15596026, USA) and reverse-transcribed into cDNA using the PrimeScript RT Kit (Takara, Cat. No. RR047A, Japan). qPCR was performed with TB Green Premix Ex Taq II (Takara, Cat. No. RR820A, Japan) on a QuantStudio 5 system (Applied Biosystems, USA). The thermal cycling conditions were as follows: 95 °C for 30 s; 40 cycles of 95 °C for 5 s and 60 °C for 30 s. Gene expression was normalized to that of β-actin and calculated using the $2^{-}\Delta\Delta Ct$ method. Primer sequences are listed in Supplementary Material 1. Three biological replicates were analyzed.

Western blot analysis

SCC-9 cells were treated with 90 μM 18β-GRA (high group) or negative control (0.05% DMSO) for 48 h. Cells were then washed with cold PBS and lysed on ice using RIPA buffer (Beyotime, Cat. No. P0013B, China) supplemented with protease and phosphatase inhibitor cocktails (Roche, Cat. Nos. 04693132001 and 04906837001, respectively, Switzerland). Lysates were incubated on ice for 30 min and clarified by centrifugation at 12,000×g for 15 min at 4 °C. Protein concentration in the supernatant was determined using a bicinchoninic acid (BCA) assay kit (Beyotime, Cat. No. P0010, China).

Equal amounts of protein (20–30 μg) were denatured in loading buffer by boiling for 5 min, separated by SDS-PAGE (using 10% or 15% gels as specified per target), and transferred to PVDF membranes (Millipore, Cat. No. IPVH00010, USA). Membranes were blocked and subsequently incubated overnight at 4 °C with the following primary antibodies (all from Cell Signaling Technology, USA, unless otherwise noted): Bax (Cat. No. 2772), Bcl-2 (Cat. No. 3498), LC3B (Cat. No. 12741), p62/SQSTM1 (Cat. No. 5114), PI3K p85 (Cat. No. 4292), Phospho-PI3K p85 (Tyr458)/p55 (Tyr199) (Cat. No. 4228), AKT (Cat. No. 75692), Phospho-AKT (Ser473) (Cat. No. 4060), and GAPDH (Proteintech, Cat. No. 60004-1-Ig, China). After washing, membranes were incubated for 1 h at room temperature with HRP-conjugated secondary antibodies: Anti-rabbit IgG (Cat. No. 7074) or Anti-mouse IgG (Cat. No. 7076) (both from Cell Signaling Technology, USA), diluted at 1:5000.

Protein bands were visualized using enhanced chemiluminescence (ECL) substrate (Millipore, Cat. No. WBKLS0100, USA) and imaged with a Tanon 5200 Multi chemiluminescence imaging system. Band intensities were quantified using ImageJ software (ImageJ, URL: https://imagej.nih.gov/ij/), with local background subtraction. Target protein expression levels were normalized to those of GAPDH.

TMT-based quantitative proteomics

TMT-based quantitative proteomics was performed by Shanghai Bioprofile Technology Co., Ltd. (China). Detailed methods are described as follows.

Protein digestion and peptide preparation

Cells in the negative control group and those treated with 90 μM 18β-GRA (designated as the high group) for 48 h were collected. For the negative control, wells were maintained in medium containing 0.05% DMSO. The experiment was performed with three biological replicates. Cell pellets were lysed in a buffer containing 4% SDS, 100 mM DTT, and 150 mM Tris-HCl (pH 8.0), boiled, sonicated, and centrifuged at 20,000×g for 15 min. Protein concentration was measured using a BCA assay.

Protein digestion was performed using a modified filter-aided sample preparation (FASP) protocol with 30 kDa Microcon filters (Merck Millipore, Cat. No. MRCF0R030). Proteins were reduced with 10 mM DTT at 60 °C for 30 min, alkylated with 50 mM iodoacetamide (IAA) in the dark at room temperature for 30 min, and washed three times with 8 M urea in 100 mM Tris-HCl (pH 8.5) and twice with 50 mM ammonium bicarbonate (ABC). Digestion was performed overnight at 37 °C with sequencing-grade trypsin (Promega, Cat. No. V5111) at an enzyme-to-substrate ratio of 1:50 (w/w) for 16 h. Peptide concentration was determined by absorbance at 280 nm.

TMT labeling and fractionation

For each sample, 100 μg of peptides were labeled with TMT10plex reagents (Thermo Scientific, Cat. No. 90110, USA) according to the manufacturer's protocol. Briefly, peptides were dissolved in 0.05 M TEAB (pH 8.5), mixed with TMT reagent reconstituted in anhydrous acetonitrile, and incubated at room temperature for 1 h. Reactions were quenched with 5% hydroxylamine. Labeled samples were pooled and dried.

High-pH reverse-phase fractionation was performed using an Agilent 1290 Infinity II HPLC system with a Waters XBridge BEH130 C18 column (2.1 × 150 mm, 3.5 μm). A total of 30 fractions were collected. These fractions were subsequently combined into 15 final samples using a concatenation strategy by mixing fractions in an alternating manner (i.e., combining fractions #1 and #16, #2 and #17, #3 and #18, …, #15 and #30). The pooled fractions were vacuum-dried and desalted prior to LC-MS/MS analysis.

LC-MS/MS analysis

LC-MS/MS was performed on a Q Exactive HF-X mass spectrometer (Thermo Scientific, USA) coupled to an Easy-nLC 1200 system. Peptides were separated on a home-made C18 column (75 μm × 25 cm, 2 μm particles) with a 90 min linear gradient from 2% to 35% acetonitrile in 0.1% formic acid at a flow rate of 300 nL/min. The mass spectrometer was operated in data-dependent acquisition (DDA) mode. MS settings: ESI spray voltage, 2.0 kV; capillary temperature, 320 °C; full MS scan (300–1800 m/z) at 70,000 resolution, AGC target 3e6, maximum injection time 50 ms; MS2 scans at 35,000 resolution, isolation window 1.2 m/z, HCD NCE 32%, AGC target 1e5, maximum injection time 100 ms, with a top 15 method and dynamic exclusion set to 30 s.

Data processing and analysis

Raw files were processed using Proteome Discoverer 2.4 (Thermo Scientific) against the Universal Protein Resource (UniProt) human database (release 2022_01). Search parameters: enzyme, trypsin/P; maximum missed cleavages, 2; precursor mass tolerance, 10 ppm; fragment mass tolerance, 20 ppm; fixed modifications, carbamidomethylation (C) and TMT10plex (K, peptide N-term); variable modifications, oxidation (M) and N-terminal acetylation. Peptide and protein false discovery rates (FDR) were set to 1% using a target-decoy approach. TMT reporter ions were quantified with a signal-to-noise (S/N) ratio threshold > 10. Differential expression was defined as a fold change > 1.20 or < 0.83 with a P-value < 0.05. Bioinformatics analysis included Gene Ontology (GO) and Kyoto Encyclopedia of Genes and Genomes (KEGG) enrichment (Fisher's exact test, FDR < 0.05) and protein-protein interaction (PPI) network construction using the Search Tool for the Retrieval of Interacting Genes/Proteins (STRING) database and Cytoscape.

Network pharmacology analysis

The putative molecular targets of 18β-glycyrrhetinic acid were first retrieved from the Traditional Chinese Medicine Systems Pharmacology (TCMSP) database, and corresponding gene information was confirmed using the UniProt database. Disease-associated genes related to tongue squamous cell carcinoma were collected from Online Mendelian Inheritance in Man (OMIM) (Supplementary Material 2), DrugBank (Supplementary Material 3), and GeneCards (Supplementary Material 4). Overlapping genes between the compound-related and disease-related sets were identified using a Venn diagram approach.

The compound–target interaction network was constructed in Cytoscape (version 3.9.0) to visualize the relationships between 18β-glycyrrhetinic acid and its predicted targets. Protein–protein interaction (PPI) analysis of the intersecting genes was performed using the STRING database (https://cn.string-db.org/), with a confidence threshold of > 0.4 (medium confidence). The resulting network was imported into Cytoscape for topological evaluation and visualization of major hubs.

Functional enrichment of the intersecting gene set was carried out using KEGG pathway analysis. Enriched pathways with a P-value < 0.05 were considered statistically significant, and the top pathways were plotted based on –log10(P) values.

Molecular docking

The 2D chemical structure of 18β-glycyrrhetinic acid was obtained from the PubChem database (https://pubchem.ncbi.nlm.nih.gov/). The structure was imported into ChemOffice 20.0 and converted into a 3D conformation, which was then saved in mol2 format. Protein structures corresponding to the predicted targets were retrieved from the RCSB Protein Data Bank (PDB) database (https://www.rcsb.org/). Only crystal structures with relatively high resolution (< 2.5 Å) were selected. Prior to docking, each protein was processed in PyMOL (version 2.6.0) to remove water molecules, phosphate groups, and other non-essential heteroatoms, and the cleaned structures were exported in PDB format. The ligand was subjected to energy minimization in Molecular Operating Environment (MOE) 2019. Protein structures were prepared in the same software, and potential binding pockets were identified using the site-finder module. Docking calculations were then carried out in MOE 2019, with the number of independent runs set to 50. The binding tendencies between 18β-glycyrrhetinic acid and each protein target were assessed mainly on the basis of docking scores and predicted binding energies. The resulting docking poses were examined and rendered with PyMOL (version 2.6.0) and Discovery Studio 2019.

Data analysis

In this study, n refers to the number of biological replicates, independent experiments, or samples. Numerical data are expressed as the mean ± standard deviation (SD). All statistical analyses were conducted using GraphPad Prism 7 software. Comparisons between two groups were performed with unpaired Student's t-tests, whereas comparisons among three or more groups were analyzed by one-way ANOVA. For experiments involving multiple comparisons, P-values were adjusted using the Benjamini–Hochberg false discovery rate (FDR) method. A P-value < 0.05 (or an FDR-corrected P-value < 0.05) was regarded as statistically significant. Data shown in the figures represent measured values normalized to internal controls. All statistical analyses were performed between treatment groups and the negative group based on these values.

Results

18β-GRA inhibits the proliferation and induces cell-cycle arrest in SCC-9 cells

CCK-8 assays showed that 18β-GRA significantly inhibited SCC-9 cell proliferation at concentrations ranging from 40 to 200 μM. The inhibitory effect intensified with increasing concentration and prolonged treatment duration, in a dose- and time-dependent manner (Fig. 1A, C). The IC_{50} values at 24, 48, and 72 h were 71.8 ± 3.47 μM, 62.63 ± 2.12 μM, and 57.70 ± 1.12 μM, respectively, indicating enhanced cellular sensitivity to 18β-GRA over time. Based on these dose-response curves, concentrations of 30, 60, and 90 μM were selected as low, medium, and high doses for subsequent experiments.

To investigate the mechanism underlying this antiproliferative effect, we examined the influence of 18β-GRA on cell-cycle distribution by flow cytometry. After 48 h of treatment, 18β-GRA induced a dose-dependent arrest at the G0/G1 phase, reflected by a progressive increase in the proportion of cells in G0/G1 and a corresponding decrease in S-phase cells, whereas the G2/M population showed no significant change (Fig. 1B, D; Table 1). These results indicate that 18β-GRA inhibits SCC-9 cell proliferation primarily by inducing G0/G1 phase cell-cycle arrest.

TMT-based quantitative proteomic profiling of 18β-GRA-treated SCC-9 cells

To investigate the molecular mechanisms underlying the anticancer activity of 18β-GRA, we performed TMT-based quantitative proteomic analysis on SCC-9 cells after treatment. Volcano plot visualization revealed a substantial alteration in the proteomic profile, with a clear separation of significantly upregulated and downregulated proteins following 18β-GRA exposure (Fig. 2A). This widespread modulation indicates that 18β-GRA affects multiple cellular processes.

KEGG pathway enrichment analysis of the differentially expressed proteins (DEPs) identified significant associations with several key pathways, including apoptosis, autophagy, complement and coagulation cascades, regulation of the actin cytoskeleton, nucleotide excision repair, and cholesterol metabolism (Fig. 2B). The pronounced enrichment of apoptosis and autophagy pathways aligns with our previous findings of inhibited proliferation and G0/G1 phase arrest, suggesting their potential contribution to the antitumor effects of 18β-GRA.

Subcellular localization annotation showed that DEPs were distributed across cytoplasmic, membrane, extracellular, and mitochondrial compartments (Fig. 2C, D), reflecting a broad cellular response. As the pathway analysis specifically highlighted apoptosis/autophagy and cytoskeleton regulation (Fig. 2B), we focused subsequent validation efforts on these biological processes rather than further interpreting the general compartment distribution patterns.

18β-GRA induces apoptosis and elevates intracellular ROS levels in SCC-9 cells

To validate the proteomic finding of apoptosis pathway activation, we evaluated apoptotic rates using Annexin V-FITC/PI staining and flow cytometry. In control cells, the majority were Annexin V^-/PI^-, indicating a low basal apoptotic rate. The apoptotic fraction increased slightly in the low-dose group and more substantially in the middle-dose group. High-dose treatment significantly elevated both early and late apoptotic populations compared to the control (Fig. 3A). Quantitative analysis confirmed a dose-dependent increase in total apoptosis, with significant differences observed in the middle- and high-dose groups (Fig. 3C).

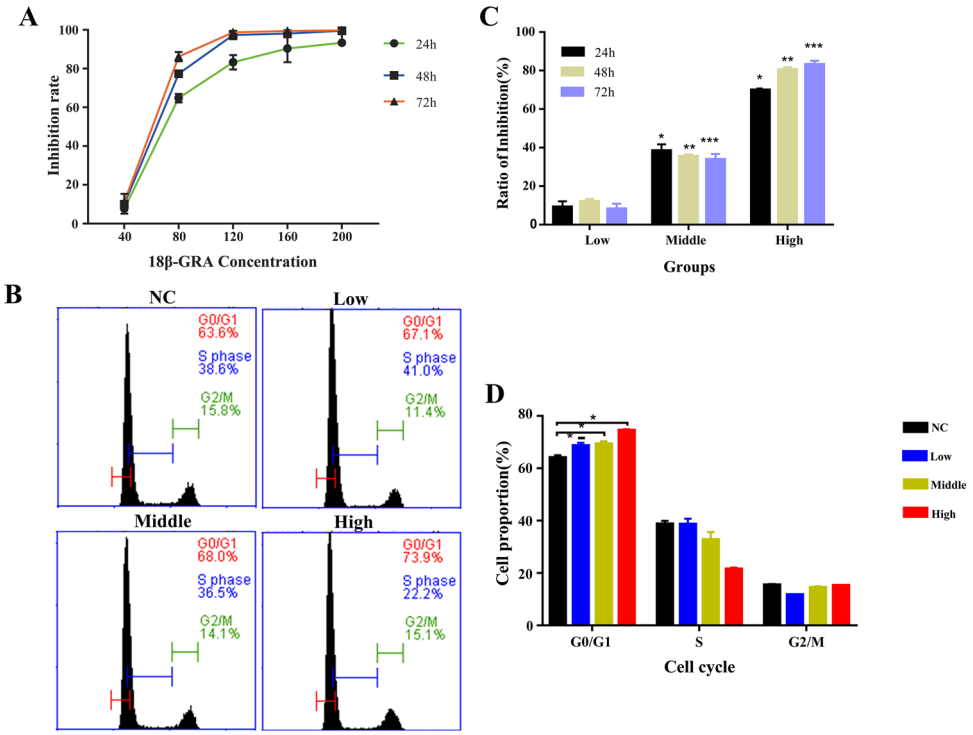

Fig. 1. 18β-GRA inhibits the proliferation and cell-cycle progression of SCC-9 cells. (**A**) Cell viability of SCC-9 cells treated with increasing concentrations of 18β-GRA for 24, 48, and 72 h was assessed using the CCK-8 assay ($n = 3$). (**B**) Representative flow cytometry histograms showing cell-cycle distribution in SCC-9 cells after exposure to low (30 μM), middle (60 μM), or high (90 μM) doses of 18β-GRA for 48 h, compared with the untreated control. (**C**) Quantification of growth-inhibition rates at low, middle, and high doses of 18β-GRA across different time points (24, 48, 72 h) ($n = 3$). (**D**) Statistical analysis of G0/G1, S, and G2/M phase proportions following 18β-GRA treatment ($n = 3$).(Data are presented as mean ± SD. ns $p \geq 0.05$, $^{*}p < 0.05$, $^{**}p < 0.01$, $^{***}p < 0.001$).

Groups	G_0/G_1phase	S phase	G_2/M phase
NC	64.06 ± 0.88	38.7 ± 1.19	15.43 ± 0.33
L	68.6 ± 1.12*	38.63 ± 2.05	11.7 ± 0.22
M	69.33 ± 0.96*	32.7 ± 2.95	14.43 ± 0.47
H	74.47 ± 0.42*	21.53 ± 0.50	15.2 ± 0.14

Table 1. Effects of 18β-glycyrrhetinic acid on the cellcCycle of SCC-9 cells. Values are presented as the mean percentage of cells in each phase (G0/G1, S, G2/M) ± standard deviation (SD).*p<0.01

We next measured intracellular reactive oxygen species (ROS) levels using the DCFH-DA fluorescent probe. Control cells exhibited minimal fluorescence, whereas high-dose 18β-GRA treatment induced a pronounced rightward shift of the fluorescence peak, indicative of elevated ROS accumulation (Fig. 3B). The mean fluorescence intensity was significantly higher in the high-dose group than in the control (Fig. 3D), confirming that 18β-GRA enhances ROS generation in SCC-9 cells.

Validation of apoptosis- and autophagy-related protein and transcript levels

To further corroborate the proteomic and functional findings, we analyzed the expression of key apoptosis and autophagy markers by Western blotting. Compared to the control, treatment with 18β-GRA upregulated the pro-apoptotic protein Bax and downregulated the anti-apoptotic protein Bcl-2 (Fig. 4A). Concurrently, 18β-GRA increased the LC3-II/LC3-I ratio, a marker of autophagosome formation, and decreased p62 levels, indicating enhanced autophagic flux (Fig. 4A).

At the transcriptional level, qPCR analysis revealed concordant changes: Bax mRNA expression was significantly increased, whereas Bcl-2 mRNA was markedly downregulated in 18β-GRA-treated cells compared to controls (Fig. 4B). These results collectively demonstrate that 18β-GRA modulates both apoptosis and autophagy pathways at the protein and gene expression levels.

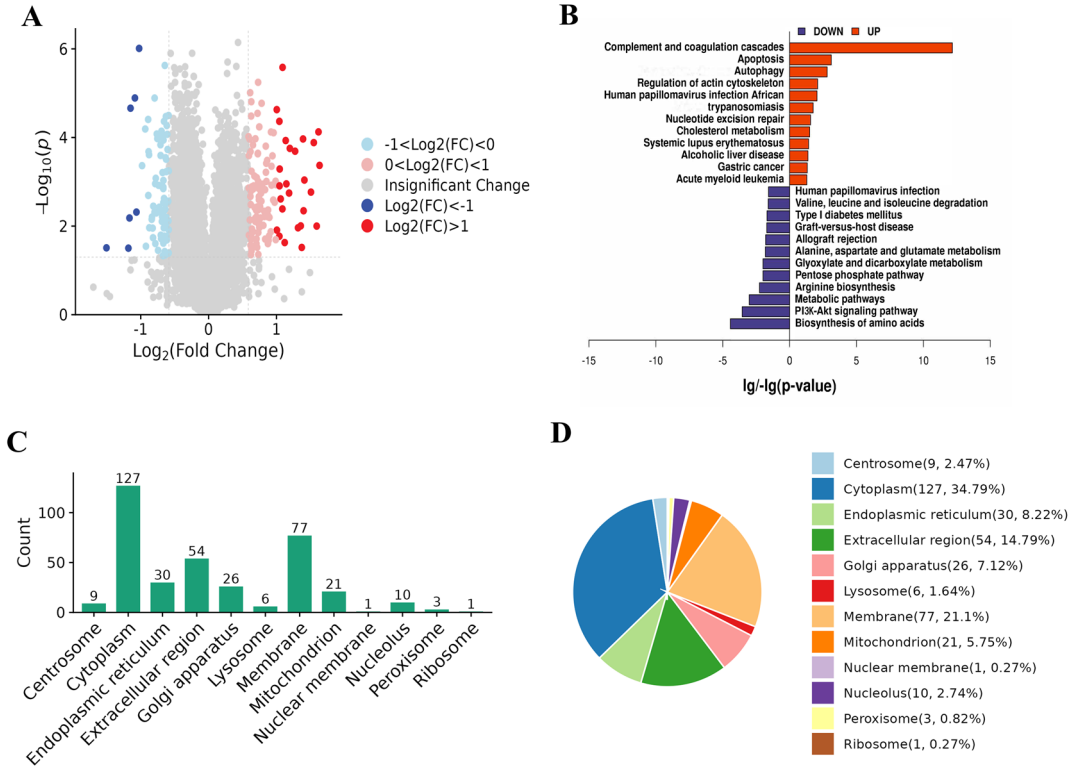

Fig. 2. TMT-based quantitative proteomic profiling of SCC-9 cells following 18β-GRA treatment. (**A**) Volcano plot showing differentially expressed proteins (DEPs) between control and 18β-GRA–treated SCC-9 cells. Proteins with significant upregulation or downregulation are highlighted (FC > 1.2 or < 0.83; $p < 0.05$).(**B**) KEGG pathway enrichment analysis of DEPs, illustrating the major upregulated and downregulated signaling pathways modulated by 18β-GRA.(**C**) Subcellular localization distribution of DEPs, classified according to functional annotations. (**D**) Pie chart summarizing the proportional distribution of DEPs across major cellular compartments.

18β-GRA inhibits PI3K/AKT signaling in SCC-9 cells

The PI3K/AKT pathway plays a critical role in promoting survival and proliferation in many epithelial cancers. Our TMT proteomic data indicated a coordinated downregulation of multiple components within this pathway. To validate this finding, we examined the expression of key signaling molecules by Western blotting. While total AKT protein levels remained unchanged between control and 18β-GRA-treated cells (Fig. 5A), the phosphorylated form (p-AKT) was markedly reduced following treatment (Fig. 5A), indicating suppression of PI3K/AKT pathway activity.

Network pharmacology and molecular docking reveal potential targets of 18β-glycyrrhetinic acid in tongue squamous cell carcinoma

To systematically explore the polypharmacological mechanisms of 18β-glycyrrhetinic acid (18β-GRA) suggested by our multi-omics data, we employed a network pharmacology approach. Potential targets of 18β-GRA were retrieved from the TCMSP database, normalized using UniProt, and used to construct a compound–target network, which displayed a radial architecture linking 18β-GRA to multiple gene nodes (Fig. 6A) .

Tongue squamous cell carcinoma (TSCC)-associated genes were collected from OMIM, DrugBank, and GeneCards. Intersection analysis between these disease genes and the predicted drug targets identified six overlapping candidates (Fig. 6B). As this preliminary overlap may include false positives, these genes were treated as putative targets for further validation. Protein–protein interaction (PPI) analysis using the STRING database revealed notable connectivity among these candidates: PTGS2, PIK3CG, HSP90AB1, PRKACA, RXRA, and PTGS1 (Fig. 6C) .

Pathway enrichment analysis of the six overlapping genes showed significant associations with xenobiotic metabolism, cancer-related pathways, and the PI3K-Akt signaling pathway (Fig. 6D). These pathways align with our proteomic results, particularly concerning metabolic and signaling dysregulation.

Molecular docking was performed to assess the binding affinity of 18β-GRA to the six hub targets. 18β-GRA fitted well into the ligand-binding pockets of all proteins, with favorable binding energies: HSP90AB1 (− 5.69 kcal/mol; Fig. 7A), PIK3CG (− 5.87 kcal/mol; Fig. 7B), PRKACA (− 6.35 kcal/mol; Fig. 7C), PTGS1 (− 6.48 kcal/mol; Fig. 7D), PTGS2 (− 6.72 kcal/mol; Fig. 7E), and RXRA (− 5.90 kcal/mol; Fig. 7F). All binding energies were below − 5.5 kcal/mol, indicating stable interactions. Notably, PTGS2 exhibited the strongest

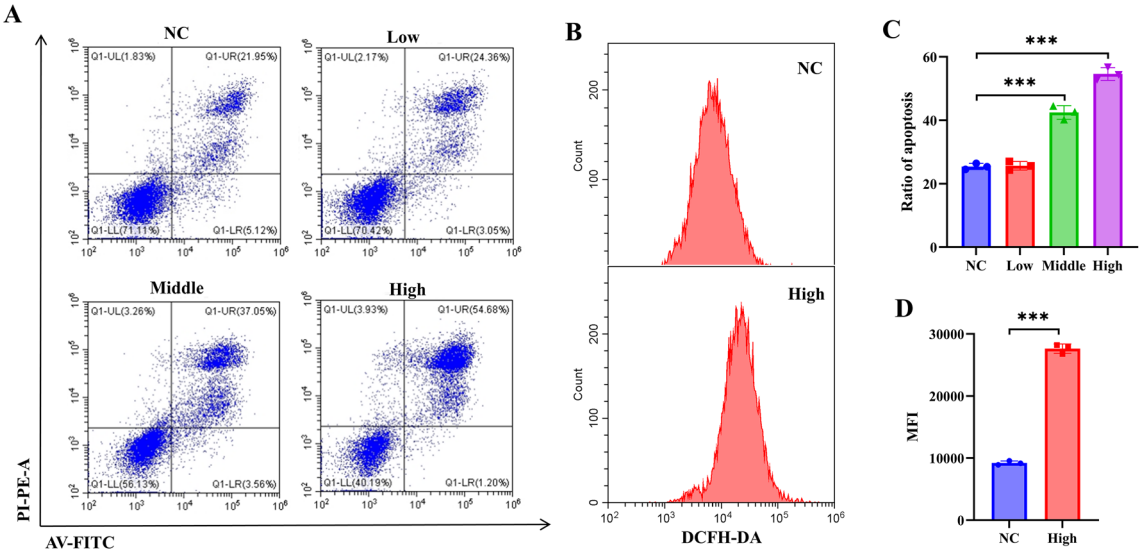

Fig. 3. 18β-GRA induces apoptosis and promotes intracellular ROS accumulation in SCC-9 cells. (**A**) Flow cytometry analysis of apoptosis in SCC-9 cells treated with low (30 μM), middle (60 μM), or high (90 μM) doses of 18β-GRA for 48 h, compared with the untreated control. Quadrant distribution reflects viable, early apoptotic, late apoptotic, and necrotic populations. (**B**) Representative DCFH-DA fluorescence histograms showing intracellular ROS levels in the control and high-dose 18β-GRA groups. (**C**) Quantitative analysis of total apoptotic cells (early + late apoptosis) across different treatment groups ($n = 3$).(**D**) Mean fluorescence intensity (MFI) of DCFH-DA, indicating changes in ROS production following high-dose treatment ($n = 3$). (Data are presented as mean ± SD. ns $p \geq 0.05$, $^{*}p < 0.05$, $^{**}p < 0.01$, $^{***}p < 0.001$).

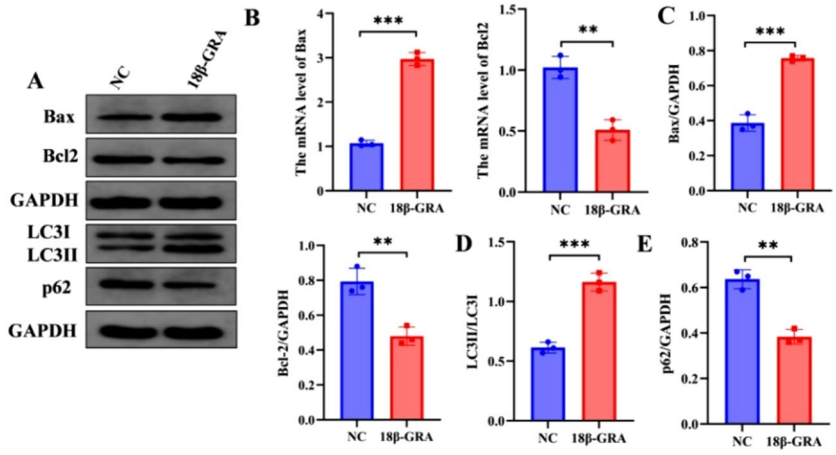

Fig. 4. Validation of apoptosis- and autophagy-related markers after 18β-GRA treatment. (**A**) Western blot analysis of apoptosis-associated proteins (Bax, Bcl-2) and autophagy-related markers (LC3-I/LC3-II and p62) in SCC-9 cells following 18β-GRA exposure (48 h). GAPDH served as the loading control.Cropped blots from three independent biological replicates are shown in Supplementary Material 7, and the raw quantification data are provided in Supplementary Material 5. (**B**) qRT-PCR quantification of Bax and Bcl-2 mRNA expression in control and 18β-GRA–treated cells ($n = 3$).(**C**) Quantification of Bcl-2 and Bax protein expression (normalized to GAPDH) in each group ($n = 3$).(**D**) Quantification of LC3-II/LC3-I ratio ($n = 3$).(**E**) Quantification of p62 protein levels relative to GAPDH ($n = 3$).(Data are presented as mean ± SD. ns $p \geq 0.05$, $^{*}p < 0.05$, $^{**}p < 0.01$, $^{***}p < 0.001$).

binding affinity, followed by PTGS1 and PRKACA, suggesting that the cyclooxygenase-2 axis may be a primary target of 18β-GRA in TSCC.

Discussion

Tongue squamous cell carcinoma (TSCC) is driven by dysregulated cell-cycle progression, impaired apoptosis, and hyperactivated oncogenic signaling pathways, underscoring the need for multi-targeting therapeutic

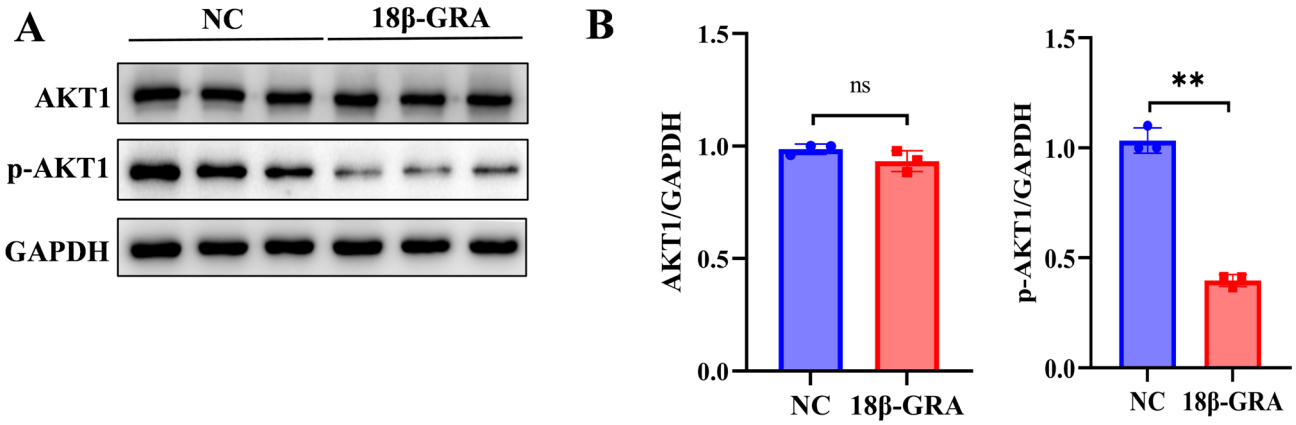

Fig. 5. 18β-GRA suppresses PI3K/AKT signaling activity in SCC-9 cells. (**A**) Representative Western blot images showing the expression of AKT1, and p-AKT1 in control (NC) and 18β-GRA–treated SCC-9 cells. GAPDH served as the loading control. (**B**) Quantification of protein levels normalized to GAPDH. Total AKT1 expression remained largely unchanged, whereas the phosphorylated forms p-AKT1 were significantly reduced following 18β-GRA exposure ($n = 3$). (Data are presented as mean ± SD. ns $p \geq 0.05$, $^{*}p < 0.05$, $^{**}p < 0.01$, $^{***}p < 0.001$).

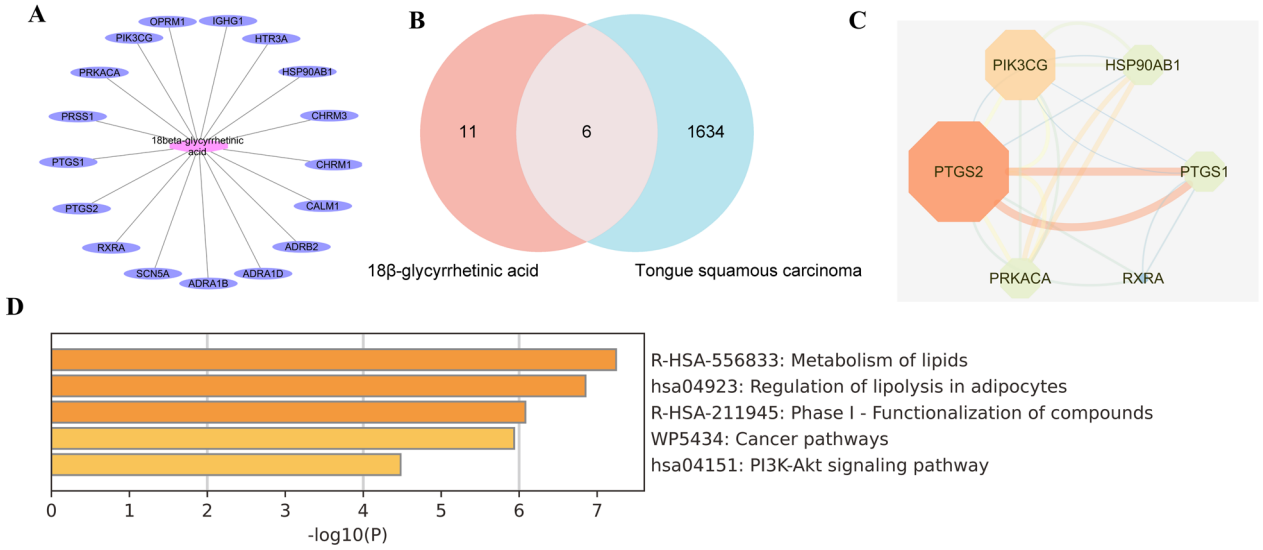

Fig. 6. Network pharmacology analysis of 18β-glycyrrhetinic acid (18β-GRA) targets and their involvement in tongue squamous cell carcinoma (TSCC). (**A**) Compound–target interaction network of 18β-GRA constructed from TCMSP and UniProt databases, illustrating multiple predicted protein targets connected to the compound.(**B**) Venn diagram showing the overlap between 18β-GRA–related targets and TSCC-associated genes, yielding six shared genes.(**C**) Protein–protein interaction (PPI) network of the six overlapping genes generated using the STRING database, with node size reflecting network connectivity; PTGS2, PIK3CG, HSP90AB1, PRKACA, RXRA, and PTGS1 form a tightly connected module. (**D**) KEGG pathway enrichment analysis of overlapping genes, highlighting significant enrichment in lipid metabolism, regulation of lipolysis in adipocytes, phase I compound functionalization, cancer-related pathways, and the PI3K–Akt signaling pathway. (Data are presented as pathway –log10(P) values, KEGG pathway diagrams (https://www.genome.jp/kegg/, licensed on 17 December 2025) and Reactome pathway diagrams (https://reactome.org).

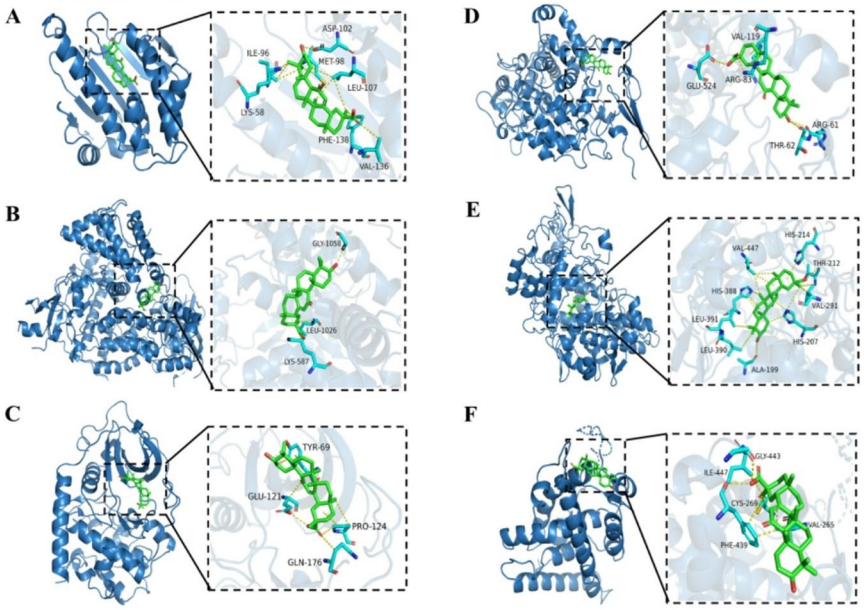

Fig. 7. Molecular docking validation of 18β-glycyrrhetinic acid with predicted core targets in tongue squamous cell carcinoma. (**A–F**) Representative docking conformations of 18β-glycyrrhetinic acid (green) bound to six intersection targets identified through network pharmacology analysis. (**A**) PTGS2, (**B**) PIK3CG, (**C**) HSP90AB1, (**D**) PRKACA, (**E**) RXRA, and (**F**) PTGS1. For each protein, the overall structure is shown on the left, and the enlarged view on the right highlights key amino-acid residues involved in hydrogen bonding or hydrophobic interactions within the predicted binding pocket.

agents[18]. Bioactive compounds derived from medicinal plants have demonstrated promising antitumor activity in TSCC and other oral cancers[19–23,35]. For instance, polysaccharides from *Ganoderma lucidum* induce G0/G1 arrest and apoptosis[19], while shikonin derivatives promote p38-mediated apoptosis[20]. Other phytochemicals, such as salidroside, asiatic acid, honokiol, and ursolic acid, modulate ERK, PI3K/AKT, and Bcl-2 signaling to inhibit viability and induce apoptosis in TSCC models[21,22]. These reports highlight the potential of plant-derived compounds as multi-target modulators in oral cancer management[23,36].

In this study, we investigated 18β-glycyrrhetinic acid (18β-GRA), a triterpenoid from *Glycyrrhiza* species with known anticancer and immunomodulatory properties[24,25,35]. Consistent with other phytochemicals, 18β-GRA suppressed SCC-9 proliferation and induced programmed cell death. The observed G0/G1 phase arrest aligns with reports that natural compounds often halt TSCC progression at pre-synthetic checkpoints, which may precede apoptotic commitment[19,21].

At the molecular level, 18β-GRA elevated the Bax/Bcl-2 ratio and increased intracellular ROS levels—a phenotype consistent with studies showing that glycyrrhetinic acid derivatives and other triterpenoids can trigger apoptosis via mitochondrial dysfunction and oxidative stress[24,26,35]. Excessive ROS can disrupt mitochondrial integrity, promote cytochrome c release, and activate caspases, ultimately driving apoptosis[27,28]. Although we did not directly assess mitochondrial membrane potential or caspase activity in this study, the observed sequence of G0/G1 arrest, ROS accumulation, and Bax/Bcl-2 imbalance closely mirrors the classical mitochondrial apoptosis pathway[27,28]. It should be noted that while ROS elevation preceded peak apoptosis in our experiments, establishing its causal role as the initiating factor will require further investigation using specific scavengers such as N-acetylcysteine (NAC) in rescue studies.

We also detected changes in autophagy markers, including an increased LC3-II/LC3-I ratio and decreased p62 levels. Similar effects have been reported for asiatic acid, honokiol, and other plant-derived compounds that modulate autophagic flux and influence tumor cell fate[21,22]. Given the context-dependent role of autophagy—which can be either cytoprotective or cytotoxic—its precise contribution to the overall response to 18β-GRA warrants further investigation[29]. Recent reviews suggest that fine-tuning the balance between autophagy and apoptosis may be key to maximizing the therapeutic efficacy of natural products in cancer[29,36].

TMT-based quantitative proteomics revealed broad alterations in pathways related to apoptosis, autophagy, metabolism, and cytoskeletal organization. Previous proteomic studies in oral and tongue cancers have highlighted the utility of high-throughput approaches for identifying functional vulnerabilities and resistance signatures[30,31,37]. Among the enriched pathways in our dataset, the PI3K–AKT cascade was particularly notable. This pathway is a well-established pro-survival axis in TSCC and is frequently hyperactivated during malignancy[32]. In our experiments, while total AKT levels remained stable, phosphorylated AKT (p-AKT) was significantly reduced following 18β-GRA treatment—consistent with reports that various phytochemicals and glycyrrhizic acid derivatives can induce apoptosis by inhibiting PI3K/AKT signaling[24,33].

Network pharmacology and molecular docking further supported the involvement of PI3K–AKT signaling. The six overlapping genes identified—PTGS2, PIK3CG, HSP90AB1, PRKACA, RXRA, and PTGS1—formed a connected protein–protein interaction module, with several nodes implicated in metabolic regulation and PI3K–AKT modulation. This multi-target profile aligns with systems-level analyses of triterpenoids in solid tumors, which often reveal convergent effects on metabolic and survival pathways[34–36]. Moreover, recent nanomedicine studies employing glycyrrhizic acid scaffolds for tumor-targeted delivery further affirm the pharmacological relevance of this chemotype in cancer therapy[35].

In summary, 18β-GRA exerts multifaceted inhibitory effects on SCC-9 cells, involving G0/G1 arrest, enhanced apoptosis, modulated autophagy, and suppression of PI3K–AKT signaling. These findings align with prior reports on plant-derived anticancer agents and multi-omics profiles in oral cancers[30,31,37], and support further investigation of 18β-GRA as a potential adjunctive therapeutic candidate for TSCC.

Limitations of the study

While this study provides insights into the potential anticancer mechanisms of 18β-GRA in TSCC, several limitations should be acknowledged.

Proteomic screening threshold

In the initial TMT proteomic screening, a relatively lenient threshold (FC ≥ 1.2 or < 0.83) was employed to maximize sensitivity for hypothesis generation. It is important to acknowledge that TMT-based quantification can be subject to ratio compression, which may lead to an underestimation of true fold changes. Consequently, the use of a 20% fold-change cutoff in the discovery phase implies that the quantified changes may be less rigorous than those obtained with larger effect sizes. However, it is important to emphasize that all key findings from this proteomic screen were subsequently validated by orthogonal experiments, including western blotting and functional rescue assays. Therefore, while the initial screening parameters were exploratory, the central conclusions of this study are firmly supported by independent experimental validation.

Model system generalizability

The findings are primarily derived from experiments using the SCC-9 cell line. Although this provides a controlled platform for initial mechanistic exploration, it limits the generalizability of the results to the broader heterogeneity of oral squamous cell carcinoma (OSCC). Future studies are warranted to validate these observations in other established OSCC cell lines (e.g., CAL-27, HSC-3), patient-derived primary cells, and in vivo models (e.g., patient-derived xenografts). Such investigations will be crucial for confirming the translational relevance of 18β-GRA across diverse OSCC contexts.

Mechanistic depth and causality

Although we observed a concomitant increase in oxidative stress and apoptosis, the experimental design does not establish a definitive causal relationship between these phenomena. Furthermore, while mitochondrial-associated apoptotic signaling was suggested by proteomic and western blot data, specific assessments of mitochondrial membrane potential and direct caspase cascade activation were not performed. Additionally, although alterations in key autophagy markers (LC3-II/LC3-I ratio, p62 levels) were detected, the precise functional role of autophagy—whether it serves a cytoprotective or cytotoxic function in response to 18β-GRA treatment—remains to be elucidated. Future functional rescue or inhibition experiments are needed to clarify these mechanistic links.

Conclusion

In summary, 18β-GRA inhibited the proliferation of SCC-9 tongue squamous cell carcinoma cells. This effect was associated with the induction of G0/G1 phase cell cycle arrest, promotion of apoptosis, modulation of autophagic markers, and suppression of the PI3K–AKT signaling pathway. Integrated proteomic and network pharmacology analyses further suggested that the anticancer activity of 18β-GRA may involve multi-target regulation across multiple biological pathways. While additional mechanistic investigations and in vivo validation are necessary, our findings provide a molecular basis for further exploring 18β-GRA as a potential therapeutic candidate for TSCC.

Data availability

The data supporting the findings of this study are available from the corresponding author upon reasonable request. The mass spectrometry proteomics data have been deposited to the ProteomeXchange Consortium (https://proteomecentral.proteomexchange.org) via the iProX partner repository[38] with the dataset identifier PXD074323.

Received: 9 December 2025; Accepted: 22 April 2026
Published online: 15 May 2026

References

1. Kim, Y. J. & Kim, J. H. Increasing incidence and improving survival of oral tongue squamous cell carcinoma. *Sci. Rep.* **10**, 7877 (2020).
2. Lenoci, D. et al. Oral cancer in young adults: Incidence, risk factors, prognosis, and molecular biomarkers. *Front. Oncol.* **14**, 1452909 (2024).
3. Katirachi, S. K., Sui, M., Wu, S., Li, Y. & Wang, B. The prevalence of HPV in oral cavity squamous cell carcinoma: A systematic review and meta-analysis. *Viruses* **15**, 2222 (2023).

4. Wu, N., Li, Y., Zhang, R., Yang, H. & Chen, S. High incidence of HPV infection in minors with oral squamous cell carcinoma. *Diagn. Pathol.* **19**, 51 (2024).
5. Kritpracha, N. et al. *Impact of Human Papillomavirus Status on Survival of Patients with Tongue Cancer: A Multicenter Cohort Study* (Heliyon, 2025) (in press).
6. Sreeram, M. P. et al. Prognostic value of primary total glossectomy in tongue cancer: A multicenter retrospective study. *Diagnostics (Basel)* (2025) (in press).
7. Gearing, P. F. et al. *Reconstruction of Tongue Malignancy Defects: A Systematic Review and Treatment Algorithm* (Microsurgery, 2025) (in press).
8. Khan, Z. et al. Functional outcomes of tongue reconstruction after oncological resection: A systematic review. *Plast. Reconstr. Surg. Glob Open* (2025) (in press).
9. Yi, C. R., Goo, E. H., Park, S. W., Lee, J. Y. & Kim, M. J. Preliminary functional outcomes and quality of life after tongue reconstruction with free flaps. *J. Reconstr. Microsurg.* **36**, 123–130 (2020).
10. Mitea, G. et al. Molecular targets of plant-derived bioactive compounds in oral squamous cell carcinoma: An update on preclinical and clinical data. *Cancers (Basel).* **16**, 534 (2024).
11. Mitea, G., Schrøder, S. A., Selescu, T., Virag, P. & Balacescu, O. Bioactive plant-derived compounds as novel chemopreventive and therapeutic agents for oral cancer. *Pharmaceuticals (Basel)* (2025) (in press).
12. Wu, Y. et al. Cardamonin suppresses proliferation and induces apoptosis of oral squamous cell carcinoma via inhibition of the PI3K/AKT pathway. *Sci. Rep.* **14**, 2187 (2024).
13. Chen, L., Gong, J., Yong, X., Li, Y. & Wang, S. A review of typical biological activities of glycyrrhetinic acid and its derivatives. *RSC Adv.* **14**, 6557–6597 (2024).
14. Shinu, P. et al. Pharmacological features of 18β-glycyrrhetinic acid: A pentacyclic triterpenoid of therapeutic potential. *Plants (Basel).* **12** (5), 1086 (2023).
15. Yuan, L. et al. 18β-glycyrrhetinic acid regulates mitochondrial ribosomal protein L35-associated apoptosis signaling pathways to inhibit proliferation of gastric carcinoma cells. *World J. Gastroenterol.* **28** (22), 2437–2456 (2022).
16. Hsu, Y. C. et al. 18β-Glycyrrhetinic acid modulated autophagy is cytotoxic to luminal A subtype breast cancer cells. *Int. J. Med. Sci.* **20**, 444–454 (2023).
17. Khalil, H. et al. Amelioration effect of 18β-glycyrrhetinic acid on methylation inhibitors in diethylnitrosamine-induced hepatocarcinogenesis. *Front. Immunol.* **14**, 1206990 (2024).
18. Jozkowiak, M. et al. Individual and combined treatments with methylated resveratrol analogue DMU-214 and gefitinib inhibit tongue cancer cells growth via apoptosis induction and EGFR inhibition. *Int. J. Mol. Sci*. **22**, 6180 (2021).
19. Li, J. et al. C.Asiatic acid induces apoptosis and cell-cycle arrest, and enhances radiosensitivity in human tongue squamous cell carcinoma SCC-15 cells via Raf/MEK/ERK signalling. *Front. Pharmacol*. 12, 690612 (2021).
20. Su, L. et al. Q.Epigenetic inhibitor AR-42 differentially affects cell cycle transit in TAZ-expressing tongue squamous cell carcinoma. *J. Cancer*. **11**, 364–373 (2020).
21. Hsu, Y. C. et al. 18β-Glycyrrhetinic acid modulated autophagy is cytotoxic to luminal A subtype breast cancer cells. *Int. J. Med. Sci.* **20**, 444–454 (2023).
22. Guo, Q. et al. 18β-Glycyrrhetinic acid inhibits non-small cell lung cancer progression by suppressing PI3K/AKT signalling and epithelial–mesenchymal transition. *Biomed. Pharmacother*. **173**, 116304 (2024).
23. Ma, C. et al. X.18β-Glycyrrhetinic acid attenuates H_2O_2-induced oxidative damage and apoptosis in intestinal epithelial cells via activation of Nrf2/HO-1 pathway. *Antioxidants* **13**, 468 (2024).
24. Cai, H., Chen, X., Zhang, J. & Wang, J. 18β-Glycyrrhetinic acid inhibits migration and invasion of human gastric cancer cells via the ROS/PKC-α/ERK pathway. *J. Nat. Med.* **72**, 252–259 (2018).
25. Wang, S. et al. W.18β-Glycyrrhetinic acid exhibits potent antitumor effects against colorectal cancer via inhibition of cell proliferation and migration. *Int. J. Oncol.* **51**, 615–624 (2017).
26. Ma, X. et al. 18β-Glycyrrhetinic acid suppresses Lewis lung cancer growth through protecting immune cells from ferroptosis. *Cancer Chemother. Pharmacol.* **93**, 575–585 (2024).
27. Li, W. X. et al. Application of 18β-glycyrrhetinic acid in the structural modification of natural products: A review. *Mol. Divers.* **29**, 739–781 (2024).
28. Quan, W. et al. Use of 18β-glycyrrhetinic acid nanocrystals to enhance anti-inflammatory activity by improving topical delivery. *Colloids Surf. B Biointerfaces*. **205**, 111791 (2021).
29. Zuo, Z., He, L., Duan, X., Peng, Z. & Han, J. Glycyrrhizic acid exhibits strong anticancer activity in colorectal cancer cells via SIRT3 inhibition. *Bioengineered* **13**, 2720–2731 (2022).
30. Hsu, P. C. & Hsu, Y. C. Therapeutic targeting of apoptosis, autophagy and necroptosis in oral cancers. *Biomedicines* **13**, 1745 (2025).
31. Honoki, K. et al. Honokiol inhibits in vitro and in vivo growth of oral squamous cell carcinoma through induction of autophagy via the PI3K/Akt and mTOR pathways. *J. Cell. Mol. Med.* **22**, 1894–1908 (2018).
32. Conlon, G. A. & Murray, G. I. Recent advances in understanding the roles of matrix metalloproteinases in tumour invasion and metastasis. *J. Pathol.* **247**, 629–640 (2019).
33. Abdel-Hamid, N. M. & Abass, S. A. Matrix metalloproteinase contribution in management of cancer proliferation, metastasis and drug targeting. *Mol. Biol. Rep.* **48**, 6525–6538 (2021).
34. Ganesh, K.J. Targeting metastatic cancer. *Nat. Med*. **27**, 34–44 (2021).
35. Gerstberger, S., Jiang, Q. & Ganesh, K. Metastasis. *Cell* **186**, 1564–1579 (2023).
36. Hebert, J. D., Neal, J. W. & Winslow, M. M. Dissecting metastasis using preclinical models and methods. *Nat. Rev. Cancer*. **23**, 391–407 (2023).
37. de Visser, K. E. & Joyce, J. A. The evolving tumor microenvironment: From cancer initiation to metastatic outgrowth. *Cancer Cell* **41**, 374–403 (2023).
38. Ma, J. et al. iProX: An integrated proteome resource. *Nucleic Acids Res.* **47** (D1), D1211–D1217 (2019).
39. Chen, T. et al. iProX in 2021: Connecting proteomics data sharing with big data. *Nucleic Acids Res.* **50** (D1), D1522–D1527 (2022).

Author contributions

Author Contributions: Hongli Fan: performed Western blot and qPCR experiments, conducted proteomic data analysis and network pharmacology analysis, organized the data, and drafted the manuscript. Daichang Yuan: carried out the in vivo experiments and prepared the figures. Yi Nan: conceptualized and designed the experiments, provided technical guidance, and critically revised the manuscript for important intellectual content.

Funding

This research was supported by the Ningxia Natural Science Foundation Project (Grant No. 2022AAC03179).

Declarations

Competing interests
The authors declare no competing interests.

Additional information
Supplementary Information The online version contains supplementary material available at https://doi.org/10.1038/s41598-026-50655-3.

Correspondence and requests for materials should be addressed to Y.N.

Reprints and permissions information is available at www.nature.com/reprints.

Publisher's note Springer Nature remains neutral with regard to jurisdictional claims in published maps and institutional affiliations.